BULLETIN OF THE POLISH ACADEMY OF SCIENCES
TECHNICAL SCIENCES, Vol. 66, No. 4, 2018
DOI: 10.24425/123928

# Single-domain nanoparticle magnetic power losses calibrated with calorimetric measurements

A. MIASKOWSKI[1*], B. SAWICKI[2], and M. SUBRAMANIAN[3]

[1] University of Life Sciences in Lublin, Department of Applied Mathematics and Computer Science, 13 Akademicka St., 20-950 Lublin, Poland
[2] Warsaw University of Technology, Faculty of Electrical Engineering, 75 Koszykowa St., 00-662 Warszawa, Poland
[3] Department of Bioengineering and Department of Computing, Royal School of Mines, Imperial College London, London, SW7 2AZ, United Kingdom

**Abstract.** The purpose of this study was to establish a numerical model for calorimetric measurements of magnetic fluids under an alternating magnetic field (AMF). The modified linear response theory (LRT) and Stoner-Wohlfarth theory were applied to investigate heat dissipation from the ferrofluid. The hysteresis area was calculated once the magnetic field value, applied frequency and number weighted distribution of the nanoparticles were known. Magnetic field distribution was calculated for the setup used for performing calorimetric experiments, and field dependent relaxation times were employed to calculate the specific loss power (SLP) in the sample. Subsequently, the results of numerical investigation were compared with the measurements obtained from calorimetric experiments. The Zeeman energy condition was used to delimit the area where LRT is valid. The numerical model calibrated with the calorimetric measurements allowed for the diffusion coefficient and the parameters involved in power dissipation in a ferrofluid to be determined. These parameters were then used to compute total heat dissipation and temperature distribution within the sample. The numerical model matching the calorimetric measurements of heat dissipation from ferrofluids enhanced the reliability of simulations.

**Key words:** magnetic fluid hyperthermia, calorimetric experiment, magnetic field, numerical modelling.

## 1. Introduction

Heat generated by magnetic nanoparticles when exposed to an alternating magnetic field has the potential to be uses as cancer treatment. This technique, known as magnetic fluid hyperthermia (MFH), has undergone and is currently going through clinical trials, and some developed countries are presently using this treatment on its own or in combination with other cancer therapies. Low concentrations of novel magnetic nanoparticles (MNPs) with potentially high dissipation rates have been increasingly proposed in the scientific community. *In vivo* and *in vitro* heating characteristics of MNPs differ and rely heavily on the exposed frequency ($f$) and magnetic field strength ($H$). On the other hand, their product ($fH$) has to be low to avoid the generation of eddy currents within tissues and stimulation of peripheral nerves [1]. Therefore, accurate methods to measure the heat are required. The heating competency of MNPs is usually quantified by the specific loss power (SLP), which is an extrinsic parameter estimated on the basis of real calorimetric measurements. SLP can be defined as the thermal power per unit mass dissipated by the magnetic material. Most studies use the term of specific absorption rate (SAR) rather than SLP [2]. However, it would be appropriate to use SLP for calorimetry and *in vitro* studies. Alternatively, SAR is defined as the heating power generated per unit mass of tissue when the human body is exposed to radiofrequency electromagnetic field, which can be associated with mobile phones, MRI scanner exposure and ultrasound.

Many factors affect MNPs' calorimetry measurements. It has been shown that the sample volume, sample container geometry, thermal properties of the container, temperature probe positioning non-uniformities in the magnetic field induced by the sample and coil geometry along with the cooling effects inside water-cooled inductors may all influence the reported SLP value [3–9]. That is why the experimental conditions under which reliable measurements of SLP may be performed in a non-adiabatic system were reviewed and quantified, aiding standardization of the technique [2, 9]. Moreover, attention was also paid to the analytical models and methods used to extract the SLP from calorimetric non-adiabatic measurements. Widely used methods to calculate SLP include the initial slope method, decay method, corrected slope method and Box-Lucas method [4, 8].

However, the literature lacks numerical models which could be used to correlate the SLP values received from measurements with computer modelling. First of all, it is necessary to clearly understand the primary parameters responsible for heat dissipation in order to effectively engineer the MNPs and experimental setup. Numerical calculations will allow us to understand and evaluate the mechanisms involved, which in turn will aid tailoring the synthesis of MNPs with optimum properties for a specific set of experimental or treatment conditions.

*e-mail: arek.miaskowski@up.lublin.pl

Manuscript submitted 2017-11-09, revised 2018-01-30, initially accepted for publication 2018-02-03, published in August 2018.

Theoretical analysis based on computer simulation of the energy converted into heat involves considering the aforementioned variables connected with the calorimetric system as well as mechanisms behind heat generation in the ferrofluids. In recent years, linear response theory (LRT) has been evaluated and modified for hysteresis losses modelling considering the importance of the dispersity index, the nanoparticle anisotropy constant and internal magnetic structure [10–14]. It was also suggested that relaxation times depend on amplitude of the external magnetic field [15–17]. Therefore, bearing in mind the polydisperse character of MNPs in the ferrofluid, it is very important to correlate the magnetic field amplitude used and maximum particle size up to which the LRT can be applied. For larger single-domain MNPs, the relaxation time lengthens and such MNPs can be regarded as blocked ones. Their behavior in an alternating magnetic field can be explained based on the Stoner-Wohlfarth theory [17–19].

To calibrate calorimetric measurements with computer modelling, the heat flow problem must be solved. In this case, the heat source plays a crucial role, and it is determined by the physical properties of MNPs, their spatial distribution, the spatial distribution of magnetic field amplitude and its frequency as well as structure and water cooling of the excitation coil [7]. Moreover, to solve the heat transfer equation, special attention should be paid to its coefficients and the boundary conditions, especially when dealing with non-adiabatic systems. However, this can be overridden by the numerical model presented in this study. A magneto-quasistatic algorithm was employed [20], and the modified LRT and Stoner-Wohlfarth theory were combined to explore the power losses due to the eddy currents, superparamagnetism and ferromagnetism. The numerical model developed can calibrate the temperature measurements from the calorimetric experiment performed but it is also flexible enough to model other complicated objects. Understanding the complications and requirements, the study presented herein aims to contribute to the standardization and validation of MNPs calorimetry.

The proposed numerical model is based on the assumption that the magnetic nanoparticles in the sample are magnetically isolated and their spatial distribution is known. The model includes 3-D distribution of the magnetic field and its heterogeneity. Those are often excluded, for simplicity although they affect both the power dissipation and temperature distribution, as it is shown in the paper. Furthermore, the magnetic field dependent relaxation times were successfully implemented in the model along with physical properties of the calorimetric system.

It is worth noting that reliability of the numerical simulation results relies on input parameters, and the aforementioned parameters are very important when dealing with complicated processes such as magnetic fluid hyperthermia. The purpose of this study is to establish a trustworthy numerical model that correlates with real calorimetric measurements. The methodology used along with theoretical modelling is presented in Sec. 2. The temperature measurement setup is presented in Sec. 3. The main results are discussed in Sec. 4, where the correlation between the final simulation results and calorimetric measurements is shown.

## 2. Materials and methods

The image of the temperature for the ferrofluid placed in the varying magnetic fields depends on the heat generation and thermal diffusivity. The theories for these two factors, applied to the calorimetric experiments, are described in the following section.

**2.1. Hysteresis area of polydisperse magnetic nanoparticles.** Assuming that the MNPs in the sample are polydisperse [11, 17] and their distribution, acquired from transmission electron microscope (TEM) analysis is a log-normal number weighted distribution, i.e. $g(d_0, s, D_\mathrm{M})$, where $d_0$, $s$ and $D_\mathrm{M}$ stand for median particle size, standard deviation and magnetic diameter of the MNP used, respectively, it is important to consider their proportion in the total volume. Therefore, the volume weighted distribution, $g(d_0, s, V_\mathrm{M})$, should be considered, as the investigated effects and properties are generally volume-dependent. In this case, $g(d_0, s, V_\mathrm{M})$ will be shifted towards larger diameters, as shown in Fig. 1, where the dashed line indicates the number weighted distribution and the solid line indicates the volume weighted distribution. For spherical nanoparticles, the volume weighted distribution can be defined as [17]:

$$g(d_0, s, V_\mathrm{M}) = \frac{g(d_0, s, D_\mathrm{M}) D_\mathrm{M}^3}{\int_0^\infty g(d_0, s, D_\mathrm{M}) D_\mathrm{M}^3 \mathrm{d}D_\mathrm{M}}. \tag{1}$$

Moreover, it is crucial to identify a suitable theory for describing the hysteresis loops of the polydisperse MNPs applied, i.e. the Stoner-Wohlfarth model based theories or the LRT, which is based on the Néel-Brown relaxation time.

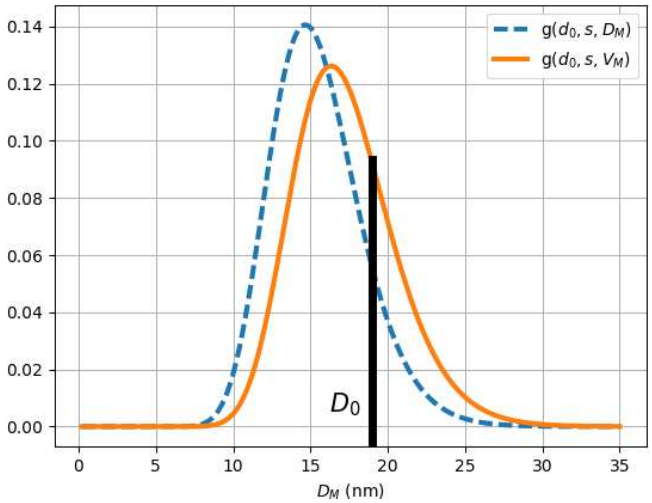


Fig. 1. Number weighted (dashed line) and volume weighted (solid line) distribution in the sample. $D_0$ (black line) indicates the maximum particle size for which the LRT can be employed; for greater diameters, the Stoner-Wohlfarth model was used ($D_0$ limit is not sharp)

For relatively large single-domain particles, i.e. under a ferromagnetic regime, the relaxation time lengthens, and such particles cannot be considered superparamagnetic, but rather blocked. The behavior of these particles can be explained using the Stoner-Wohlfarth model based theories. Alternatively, assuming that the smaller MNPs are under a superparamagnetic regime, the LRT can be used. Thus, it is important to determine the critical diameter ($D_0$) that delimits the application of both theories.

The main assumption in the LRT is that the Langevin function remains linear for the maximum field used in the experiments. To satisfy this condition, thermal energy has to dominate over Zeeman energy [17]:

$$\frac{\mu_0 \mu H_{\max}}{k_B T} < 1, \tag{2}$$

where $k_B$ is the Boltzmann constant, $T$ is the temperature, $H_{\max}$ is the maximum magnetic field strength amplitude, $\mu$ is the magnetic moment of the superparamagnetic particle defined as $\mu = M_s V_M$, where $M_s$ stands for saturation magnetization and $V_M$ stands for magnetic volume of the nanoparticle ($\pi D_M^3/6$).

When MNPs in the superparamagnetic regime are exposed to an AMF with the given parameters ($H_{\max}$, $f$), the magnetization lags behind the external field, and heat dissipation in W/kg can be expressed as the specific loss power [15]:

$$\mathrm{SLP_{LRT}} = \int_0^{V_0} \pi \mu_0 \chi'' H_{\max}^2 f (\rho V_M)^{-1} g(d_0, s, V_M) \mathrm{d}V, \tag{3}$$

where $V_0$ is the volume of MNP having diameter $D_0$ (see Fig. 1), $\rho$ is the density and $\chi''$ is the average out-of-phase component of susceptibility given by [19, 22]:

$$\chi'' = \frac{\mu_0 \mu}{3 k_B T} \frac{2\pi f \tau}{1 + (2\pi f \tau)^2}, \tag{4}$$

where $\tau$ is the Néel-Brown relaxation time. The Néel ($\tau_N$) and Brownian ($\tau_B$), as dependent on external magnetic field ($H$), are obtained from [16, 17]:

$$\frac{1}{\tau_N(H)} = f_0 (1 - h^2) \left\{ (1+h) \exp\left[ \left( -\frac{K V_M}{k_B T} \right) (1+h)^2 \right] + (1-h) \exp\left[ \left( -\frac{K V_M}{k_B T} \right) (1-h)^2 \right] \right\}, \tag{5}$$

$$\frac{1}{\tau_B(H)} = \tau_B^{-1} \left( 1 + 0.07 \left( \frac{\mu_0 \mu H}{k_B T} \right)^2 \right)^{0.5}, \tag{6}$$

where $\tau_B = (3\eta V_H)/(k_B T)$, $h = H/H_k$ and $\mu_0 H_k = 2K/M_s$ represents the anisotropy field with anisotropy constant $K$, while $V_H$ is the hydrodynamic diameter of MNP, $\eta$ is the viscosity, $T$ is the temperature and $f_0 = 10^9$ s$^{-1}$ is the so-called Larmor frequency or otherwise the inversion of Larmor time $\tau_0$ ("the measure time") [10, 22]. The existence of two relaxation times leads to the effective relaxation time given by $\tau(H)^{-1} = \tau_N(H)^{-1} + \tau_B(H)^{-1}$. In the case of randomly oriented easy axes, the cumulative effect of particles with different orientations lowers the coercive field to 0.48 $\mu_0 H_k$ and suppresses the remanence to half of the saturation value. The area of the hysteresis loop is then $2\mu_0 M_s V_M = 0.96\ \mu_0 M_s V_M H_k$ [17].

Above a critical diameter ($D_0$, see Fig. 1), which can be determined from the Zeeman condition (1), the magnetic nanoparticles will be blocked, and their contribution to heating must be calculated outside the scope of the LRT model. In this case, the coercive ($H_c$) field was given by [19]:

$$H_c = H_k (1 - \kappa^{1/2}) \tag{7}$$

with the following dimensionless parameter:

$$\kappa = \frac{k_B T}{K V_M} \ln\left( \frac{k_B T}{4 \mu_0 \tau_0 H_{\max} M_s V_M f} \right). \tag{8}$$

Finally, taking into account the Zeeman energy condition together with the volume weighted distribution, the specific power losses (W/kg) for the Stoner-Wohlfarth model can be presented as [11]:

$$\mathrm{SLP_{SW}} = 2\mu_0 M_s f \rho^{-1} \int_{V_0}^{\infty} H_c(V_M) g(d_0, s, V_M) \mathrm{d}V. \tag{9}$$

**2.2. Heat transfer equation.** Distribution of temperature ($T$) is described by the heat transfer partial differential equation [2, 22]:

$$\rho c \frac{\partial T}{\partial t} = \nabla \cdot (k \nabla T) + \mathrm{SLP_{ext}} \rho_{\mathrm{ferrofluid}}, \tag{10}$$

where $\rho$ is the density of the material (kg/m), $c$ is the specific heat parameter (J/kg/K), $k$ is the thermal conductivity (W/m/K), and the product of $\mathrm{SLP_{ext}}$ and $\rho_{\mathrm{ferrofluid}}$ is the external power density generated in the sample (W/m$^3$). However, the steady state solution and the curvature of the heating curve are mainly determined by the boundary condition together with the material properties used during the experiments [23]. For the description of the heat exchange with the surrounding environment, the convection phenomena formulation has been used:

$$k \frac{\partial T}{\partial n} = h\,(T_{\mathrm{ext}} - T)\,, \tag{11}$$

where $h$ is the heat transfer coefficient, which is specific for the external surface of the model, and $T_{\mathrm{ext}}$ stands for external air temperature. The same value is used as an initial boundary condition, $T(t = 0) = T_{\mathrm{ext}}$.

Solution of (10) with boundary condition (11) requires knowledge of the geometry of the model, which can be measured, as well as all other parameters of the model. Some of these measurements can be taken from the literature, and others can be obtained from producer specifications. That is why the most important objective of this paper is to confirm the value of the MFH source, $\mathrm{SLP_{ext}}$, which can be received from calorimetric measurements.

## 3. Calorimetric experiments

For the calorimetric experiments, 2 mL of 5 mg/mL concentrations of dimercaptosuccinic acid (DMSA) stabilized

magnetite nanoparticles (HyperMAG, Liquids Research, Bangor, UK) were used with 2 mL graduated temperature and pressure-resistant vials (Nalgene, Thermo Fisher Scientific, New York, USA). MNPs were vortexed and ultra-sonicated prior to calorimetry. A temperature sensor was positioned in the center of the ferrofluid sample. The Osensa FTX-200-LUX+ optical temperature sensor system (British Columbia, Canada) was used for real-time temperature measurement, while subjecting the sample to a 9-turn helical coil with 50 mm inner diameter attached to the magneTherm system (nanoTherics, Staffordshire, UK), similar to that described in [2]. The MNP sample ($H_{\max} = 10.3$ kA/m) was investigated, in the middle of the excitation coil, at $f_1 = 171$ kHz and $f_2 = 257$ kHz. The measurements were repeated three times for the sample.

If the perfect adiabatic condition is valid, the amount of heat generated in the sample was quantified in terms of the specific loss power, SLP (W/g of the particles), and calculated as [4]:

$$\text{SLP} = \frac{C}{\varphi}\frac{\Delta T}{\Delta t}, \tag{12}$$

where the specific heat capacity of the ferrofluid is $C$ (J/K/mL), the concentration of MNPs is $\varphi$ (mg/mL), and the rate of change of temperature over time is $\Delta T/\Delta t$. An appropriate region of the graph was used for the calculations using the corrected slope method [4]. This method corrects the value determined by the (initial) slope method for any linear losses already apparent at that temperature of $(P = C(\Delta T/\Delta t) + L\Delta T)$.

When the value of thermal loss $L$ of the system is known, the SLP can be calculated using [4]:

$$\text{SLP}_{\text{corrected-slope-method}} = \left(C\frac{\Delta T}{\Delta t} + L\Delta T\right)/m_{\text{MNP}}. \tag{13}$$

In (12), $\Delta T$ is the mean temperature difference between the sample and baseline, which will be within the bounds of the linear-loss regime. When the loss $L$ is not known, as it is hard to accurately measure all the parameters involved, it is possible to estimate the linear loss parameter from the temperature difference over time slope, based on the fitting interval and number of fits.

## 4. Results and discussion

The calorimetric experiments described in the previous section are the foundation of numerical evaluation. The laboratory setup was reconstructed using computer software with precisely the same geometry and magnetic field source. Numerical results aid the investigation of the heating process.

**4.1. Numerical model of experimental setup.** The numerical model of the setup, including the materials which are often excluded, is shown in Fig. 2. In this case, the volume of the Eppendorf tube with the magnetic fluid sample was 2 mL, the volume of air was 1.14 mL, and the volume of the Styrofoam was 100.5 mL. In this manner, the worst-case scenario of having some inner air inside the Eppendorf tube was considered. Finally, the three-dimensional model, suitable for the finite element method, was generated.

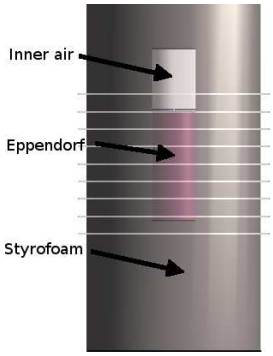


Fig. 2. CAD model of experimental setup

The physical properties of the materials of the magneTherm system in Fig. 2 ($\rho_s$, $c_s$, $k_s$, i.e. density, specific heat capacity as well as thermal conductivity, respectively) used to solve (10) were obtained from [21]. The properties of the ferrofluid in the Eppendorf sample that were calculated as being effective [2, 21] are summarized in Table 1.

Table 1
Physical properties of materials used in the numerical model (see Eq. (10)) [2, 21]

| Material | $\varrho$ [kg/m$^3$] | $c$ [J/kg/K] | $k$ [W/m/K] | $\sigma$ [S/m] |
|---|---|---|---|---|
| Styrofoam | 15.0 | 1200.0 | 0.16 | 0.00047 |
| Eppendorf tube | 946.0 | 1920.0 | 0.35 | 0.0005 |
| Water | 998.0 | 4178.0 | 0.6 | 0.00005 |
| Magnetite | 5180.0 | 670.0 | 9.7 | $25.0{\cdot}10^3$ |
| Ferrofluid | 998.07 | 4174.6 | 0.6 | $5.00483{\cdot}10^{-5}$ |
| Air | 1.16 | 1003.67 | 0.0274 | – |

**4.2. Magnetic field distribution in the system.** To numerically investigate the magnetic field distribution in the magneTherm$^{\text{TM}}$ system, numerical simulation software with the low frequency magnetoquasistatic solver was applied (Sim4Life, ZMT Zurich MedTech AG, Switzerland). The magnetostatic vector potential ($\mathbf{A}_0$) is calculated over the current density domain $\Omega$, by means of the Biot-Savart law:

$$\mathbf{A_0}(r) = \frac{\mu_0}{4\pi}\int\limits_{\Omega}\frac{\mathbf{J}_0(\mathbf{r}')}{|\mathbf{r}-\mathbf{r}'|}\mathrm{d}^3\mathbf{r}', \tag{14}$$

where $\mathbf{J}_0$ stands for the given current density vector. For the modeled case of low-frequency stimulation, conductivity ($\sigma$) is much greater than the product of permittivity ($\varepsilon$) and angular frequency ($\omega$), i.e. $\sigma \gg \omega\varepsilon$, so one can solve the following equation:

$$\nabla\cdot\sigma\nabla\phi = -\mathrm{j}\omega\nabla\cdot(\sigma\mathbf{A}_0), \tag{15}$$

where $\phi$ is the electric scalar potential. The electric field is calculated only in the loss domain ($\sigma \neq 0$), whereas the magnetic field strength, $\mathbf{H}$, is calculated everywhere ($\mathbf{H} = \mu_0^{-1}\nabla\times\mathbf{A}$).

In our numerical investigation, the amplitude of the current in the 9-turn coil was $I_m = 64.36$ A, and the wire radius was $r = 2.5$ mm. The magnetic field strength distribution

($H_{\max}$) can be seen in Fig. 3, in which the positions of the materials and corresponding properties from Fig. 1 and Table 1 with relation to the coil were included. Figure 3 depicts the $H_{\max}$ distribution without the sample (magnetic fluid is not included), and Fig. 4 displays a magnetic field along the $x$- and $z$-axis, both indicated with green lines. It is evident that the magnetic field strength distribution is highly heterogeneous in the sample volume, ranging from 0.8 kA/m to 10.3 kA/m. This magnetic field can be viewed as the working one, i.e. it represents the input parameter, while (3), (9) and (10) represent the response of the system to the alternating magnetic field.

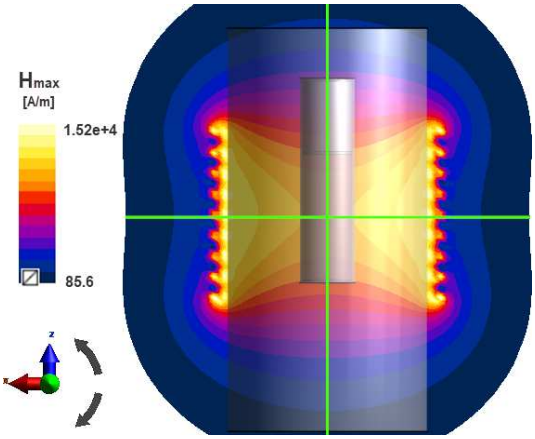


Fig. 3. Magnetic field strength amplitude ($H_{\max}$) inside 9-turn coil ($xz$-cross section), $I_{\mathrm{m}} = 64.36$ A, and wire radius $r = 2.5$ mm

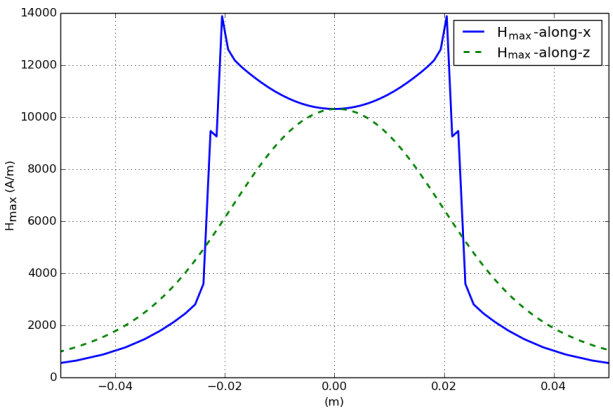


Fig. 4. Magnetic field strength amplitude in the middle of the system coil along the $x$- and $z$-axis ($I_{\mathrm{m}} = 64.36$ A, wire radius $r = 2.5$ mm)

**4.3. Single-domain particle magnetic power losses.** To numerically investigate the magnetic power losses, the model introduced in (3)–(9) was implemented. The calculations were completed for two different frequencies, $f_1 = 171$ kHz and $f_2 = 257$ kHz, at the same magnetic field as per the experimental conditions. In addition to the physical parameters of the MNPs provided in Table 1, the following data were used: saturation magnetization $M_{\mathrm{s}} = 92$ kA/m, $\tau_0 = 10^{-9}$ s, the anisotropy constant equal to $K = 30$ kJ/m$^3$, Boltzmann constant $\mathrm{k_B} = 1.38 \times 10^{-23}$ J/K, $\varphi = 5$ kg/m$^3$ and temperature $T = 300$ K. These all correspond to magnetite physical properties. To calculate the Brownian relaxation time, the viscosity of water, $\eta = 8.94 \times 10^{-4}$ kg/m/s, and the surfactant layer thickness, $\delta = 2$ nm, were set together with $d_0 = 15.2$ nm and $s = 0.19$, which were set in the lognormal density distribution function, i.e. $g(d_0, s, V_{\mathrm{M}})$. Moreover, as stated above, the concentration of the nanoparticles in the sample does not exceed 5 mg/mL, so the effects caused by dipole-dipole interactions between the nanoparticles were considered insignificant at room temperature. Thus, in our case, the nanoparticles were considered to be magnetically isolated from each other.

The results of the calculations are shown in Fig. 5 (for better visualization, the data were rescaled and minimum power was set at $5 \times 10^4$ W/m$^3$ for 171 kHz and at $10^6$ W/m$^3$ for 257 kHz). It can be seen that the power is not homogeneous in the sample volume and varies from approximately 80 kW/m$^3$ to 117 kW/m$^3$ for $f_1 = 171$ kHz and from approximately 120 kW/m$^3$ to 176 kW/m$^3$ for $f_2 = 257$ kHz. In the case of frequency of 257 kHz, there are power losses of 170 kW/m$^3$ in the middle of the sample.

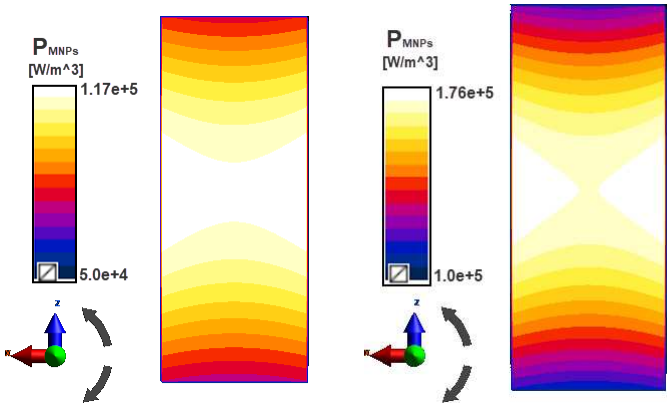


Fig. 5. Single-domain nanoparticle magnetic power losses distribution in 2mL sample (cross section) for $f_1 = 171$ kHz (left) and $f_2 = 257$ kHz; $H_{\max} = 10.3$ kA/m

The above-calculated values can easily be converted to W/g, including particle concentration ($\varphi$), to obtain the SLP range from 11.31 W/g to 16.55 W/g for $f_1 = 171$ kHz and from 16.97 W/g to 24.89 W/g for $f_2 = 257$ kHz. Finally, these values can be easy compared with those measured, i.e. SLP $= 16.27 \pm 0.8$ W/g for frequency $f_1$ and SLP $= 25.23 \pm 0.7$ W/g for $f_2$, respectively. In the first case, the maximum value was overestimated, whereas in the second, it is underestimated when compared with the experimental SLPs. Finally, due to the heterogeneous magnetic field strength in the sample volume, the power dissipation was also heterogeneous.

Subsequent sections will discuss how this magnetic field and the power losses influence temperature distribution in the sample.

**4.4. Temperature distribution in the sample.** Temperature distribution in the sample was investigated on the basis of the mathematical model (10) using transient Sim4Life thermal solver with the parameters taken from Table 1. The homoge-

nous temperature, $T(t = 0) = 25°C$, for each individual object (see Fig. 2) was specified at the start of the simulation together with external temperature $T_{ext} = 25°C$ and the mixed boundary condition with heat transfer coefficient $h = 1.5$ W/(m$^2$ K). The simulation time was $t_{max} = 1800$ s. The *xz*-cross section of temperature distribution passes through the middle of the sample after 1500 seconds of heating for the two different frequencies, as shown in Fig. 6. In the first case, the temperature reached 41.9°C, while in the second case, it reached 52.1°C. The minimum temperatures were set at 37°C in both cases in order to improve visualization. Figure 7 shows

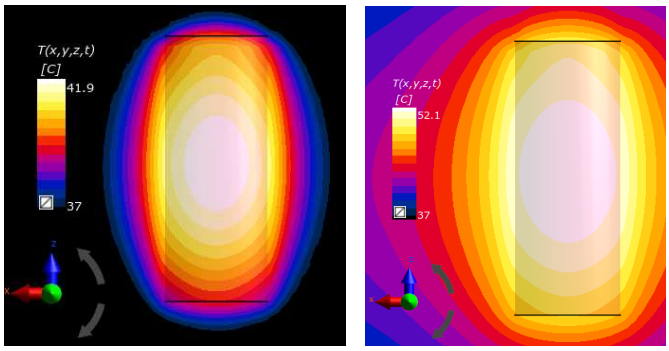


Fig. 6. Temperature distribution in 2mL sample (cross section) after 1500 seconds for $f_1 = 171$ kHz (left) and for $f_2 = 257$ kHz (right)

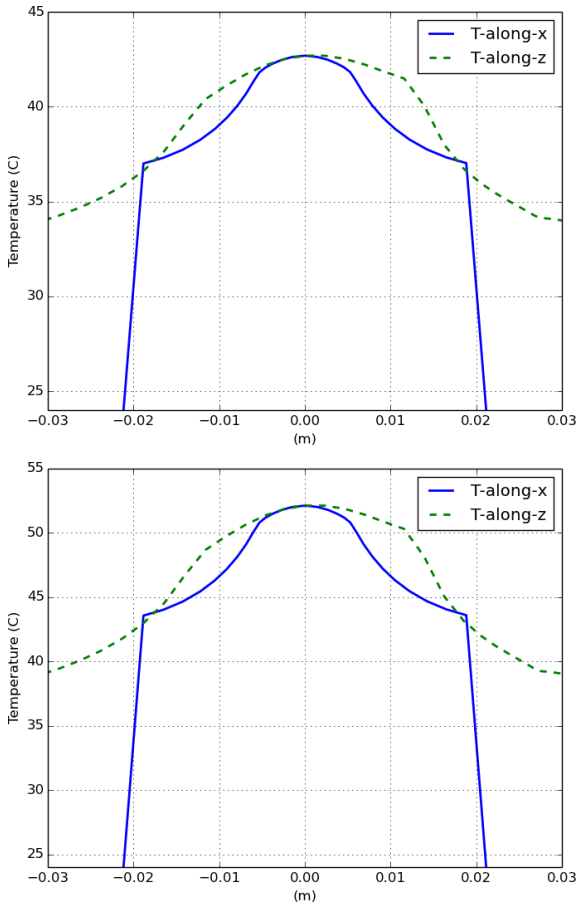


Fig. 7. Spatial distribution in 2mL sample along the $x$ and $z$-axis for $f_1 = 171$ kHz (top) and for $f_2 = 257$ kHz (bottom)

spatial distribution along the $x$- and $z$-axis for the two different frequencies. One can see that the temperature is not symmetrical due to presence of air in the upper part of the sample.

The results obtained from *in vitro* calorimetric measurements were compared with those derived from numerical analysis. The comparison is shown in Fig. 8, where the dotted line indicates the calorimetric measurements performed and the solid line indicates the calculations.

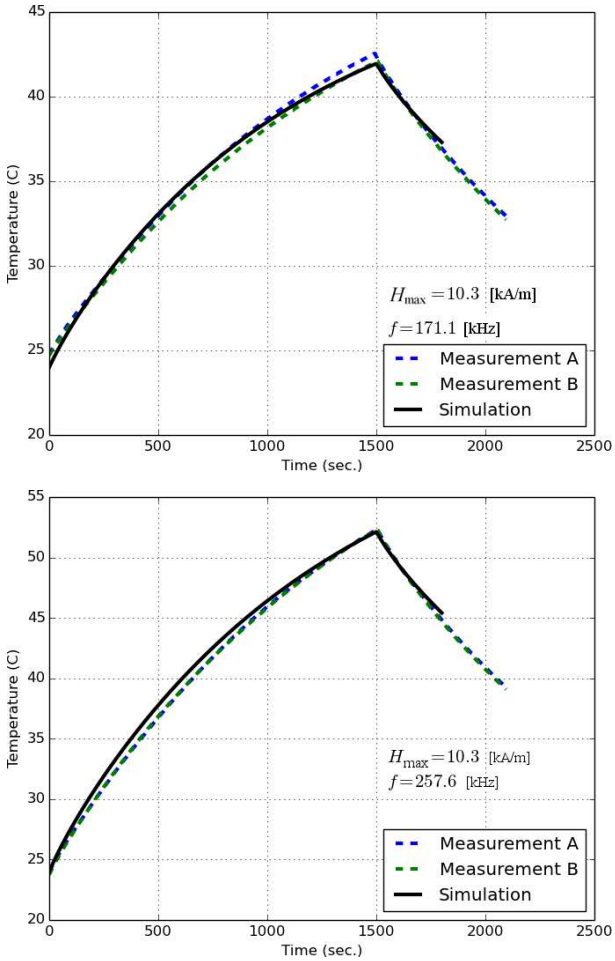


Fig. 8. Temperature as a function of time for 2mL sample for $f_1 = 171$ kHz (top) and for $f_2 = 257$ kHz (bottom), $H_{max} = 10.3$ kA/m. The calculations were conducted on the basis of (10) with parameters from Table 1. The solid line indicates the simulation, while the dotted line indicates the calorimetric measurements

It can be seen that after 1500 seconds the magnetic field was switched off and the sample started to cool down. As expected, inhomogeneous spatial distribution of temperature can be seen in the sample that was heated in the non-adiabatic system. The causes for this include steady-state diffusion and convection effects as well as inhomogeneous dissipation of heat from the sample into its environment, either from its surface or through the walls of the sample container. However, taking into account the temperature distribution in the sample due to the power loss from Fig. 6, one can conclude that the ferrofluid sample, i.e. its physical properties, fulfils

the assumption of the correctness of the mathematical model. However, there are differences in the measurements and the computer modelling prediction due to factors arising from the computer model simplifications. These include, for example, the constant value of anisotropy ($K$) and the spherical shape of the magnetic nanoparticles.

## 5. Conclusions

This study presents the 3-D numerical model of calorimetric measurements with usage of the magneTherm$^{TM}$ system. In our case, the model included the Styrofoam isolating layer, an Eppendorf tube and a ferrofluid sample. To investigate power losses in the ferrofluid, heat dissipation in the sample was calculated on the basis of combined Linear Response and Stoner-Wohlfarth theories. It was assumed that the MNPs were polydisperse and magnetically isolated. Subsequently, the heat transfer equation (10) with the Robins boundary condition (11) was solved. Finally, the results of the calculations and real calorimetric measurements were compared. The results indicated that the power losses and temperature distribution inside the ferrofluid sample were not homogenous and that measuring the temperature in the sample could lead to different values for the specific loss power. Taking into account the comparative analysis presented in this work, the correctness and reliability of the mathematical model developed were shown to be useful for *in silico* applications or during the planning of magnetic fluid hyperthermia treatment.

There is a need for better theoretical explanation and standardized protocol for performing magnetic fluid calorimetry experiments *in vitro*. In reality, the theoretical determination of losses mediated by AMF is complex and relies upon numerous parameters, rather than on the few variables considered in most research studies. It is obvious that considering more parameters will increase accuracy, but the measurement and associated human errors involved cannot be neglected. Moreover, electrostatic interactions, such as clustering and chain formation, as well as intra and inter-particle interactions are difficult to quantify and model. It should also be noted that spatial rearrangements of nanoparticles in the suspension change during AMF exposure, and the particle interactions will also change. The complex internal structure of the MNPs, i.e. multi-domain magnetic cores, can also influence SLP determination. Furthermore, the characterization of MNPs using EM accompanied by AC susceptibility losses is also important.

With the initial-slope correction method, which was used in this work in order to evaluate SLP, the sample temperature is assumed to be homogenous, and the heat losses are presumed trivial when hysteresis heating starts. The relevant literature clearly demonstrates the uncertainty behind SLP determination in experiments with long exposure times involving high ferrofluid sample concentrations, high flux density and high frequencies [3]. This encouraged us to consider the entire change of the temperature curve for each sample. Compensation for non-adiabatic conditions is necessary but is not enough to deduce errors in measurements. Most studies fail to consider the physical and geometric properties of the coil, but the coil or the sample geometry can be modified to achieve better field homogeneity and incident intensity. However, temperature distribution within the sample will still influence measurement error.

Herein, the sample tube geometry and volume of the MNP used for calorimetry were kept constant. The sample was equilibrated to the ambient temperature within the sample chamber before each run, and the temperature was observed for more than 25 seconds to note the cooling effects of the MNP samples. The experiment was repeated at least three times for each type of MNP with fresh samples. Water blank was used as a control, and the control established that there was no non-specific heating. However, a recently published study suggests minimizing the AMF exposure time period to less than 100 seconds to reduce degradation of the MNPs used when performing calorimetric experiments involving different fields and frequencies, suggesting that the topic of magnetic fluid hyperthermia is constantly evolving [9].

**Acknowledgements.** The authors wish to thank Professor Kevin O'Grady and Dr. Gonzalo Vallejo-Fernandez, University of York, UK, for providing extensive support throughout this study. We also thank Liquids Research, Ltd. for the transfer of knowledge regarding HyperMAG particles. We are grateful to Professor Jon Dobson of the University of Florida, USA, for his conversations regarding biomagnetics, and we thank nanoTherics, Ltd., Staffordshire, UK, for their aid.

REFERENCES

[1] W.J. Atkinson, I.A. Brezovich, and D.P. Chakraborty, "Usable Frequencies in Hyperthermia with Thermal Seeds", *IEEE Trans. Biomed. Eng.* 31(1), 70–75 (1984).

[2] P. Gas and A. Miaskowski, "Specifying the ferrofluid parameters important from the viewpoint of Magnetic Fluid Hyperthermia", *Selected Problems of Electrical Engineering and Electronics (WZEE)*, 1–6 (2015), DOI: 10.1109/WZEE.2015.7394040.

[3] S.Y. Wang, S. Huang, and D.A. Borca-Tasciuc, "Potential sources of errors in measuring and evaluating the specific loss power of magnetic nanoparticles in an alternating magnetic field", *IEEE Trans. Magn.* 49(1), 255–262 (2013).

[4] R.R. Wildeboer, P. Southern, and Q.A. Pankhurst, "On the reliable measurement of specific absorption rates and intrinsic loss parameters in magnetic hyperthermia materials", *J. Phys. D: Appl. Phys.* 47, 495003 (2014).

[5] S. Huang, S.Y. Wang, A. Gupta, D.A. Borca-Tasciuc, and S.J. Salon, "On the measurement technique for specific absorption rate of nanoparticles in an alternating electromagnetic field", *Meas. Sci. Technol.* 23, 035701 (2012).

[6] A. Skumiel, T. Hornowski, A. Jozefczak, M. Koralewski, and B. Leszczynski, "Uses and limitation of different thermometers for measuring heating efficiency of agnetic fluids", *Appl. Therm. Eng.* 100, 1308–1318 (2016).

[7] P. Gas and E. Kurgan, "Cooling effects inside water-cooled inductors for Magnetic Fluid Hyperthermia", *2017 Progress in Applied Electrical Engineering (PAEE)*, 1–4 (2017).

[8] A. Attaluri, C. Nusbaum, M. Wabler, and R. Ivkov, "Calibration of a quasi-adiabatic magneto-thermal calorimeter used to

characterize magnetic nanoparticle heating", *J. Nanotechnol. Eng. Med*. 4(1), 011006 (2013).

[9] F. Soetaert, S.K. Kandala, A. Bakuzis, and R. Ivkov, "Experimental estimation and analysis of variance of the measured loss power of magnetic nanoparticles", *Sci. Rep.* 7, 6661 (2017).

[10] R.E. Rosensweig, "Heating magnetic fluid with alternating magnetic field", *J. Magn. Magn. Mater.* 252, 370–374 (2002).

[11] G. Vallejo-Fernandez, O. Whear, A.G. Roca, S. Hussain, J. Timmis, et al., "Mechanisms of hyperthermia in magnetic nanoparticles", *J. Phys. D Appl. Phys.* 46, 312001 (2013).

[12] C.L. Dennis, K.L. Krycka, J.A. Borchers, R.D. Desautels, J. Van Lierop, et al., "Internal magnetic structure of nanoparticles dominates time-dependent relaxation processes in a magnetic field", *Adv. Funct. Mater.* 25, 4300–4311 (2015).

[13] G. Vallejo-Fernandez and K. O'Grady, "Effect of the distribution of anisotropy constants on hysteresis losses for magnetic hyperthermia applications", *Appl. Phys. Lett*. 103, 142417 (2013).

[14] C.L. Dennis and R. Ivkov, "Physics of heat generation using magnetic nanoparticles for hyperthermia", *Int. J. Hyperther*. 29(8), 715–729 (2013).

[15] H. Mamiya, "Recent advances in understanding magnetic nanoparticles in AC magnetic fields and optimal design for targeted hyperthermia", *J. Nanomater*. 2013, 752973 (2013).

[16] H. Mamiya and B. Jeyadevan, "Hyperthermic effects of dissipative structures of magnetic nanoparticles in large alternating magnetic fields", *Sci. Rep*. 1, 157 (2011).

[17] M. Boskovic, G.F. Goya, S. Vranjes-Djuric, N. Jovic, B. Jancar, et al., "Influence of size distribution and field amplitude on specific loss power", *J. Appl. Phys*. 117, 103903 (2015).

[18] C. Tannous and J. Gieraltowski, "The Stoner-Wohlfarth model of ferromagnetism", *Eur. J. Phys*. 29(3), 475–487 (2008).

[19] J. Carrey, B. Mehdaoui, and M. Respaud, "Simple models for dynamic hysteresis loop calculations of magnetic single-domain nanoparticles: Application to magnetic hyperthermia optimization", *J. Appl. Phys.* 109, 083921 (2011).

[20] A. Miaskowski, B. Sawicki, and A. Krawczyk, "The use of magnetic nanoparticles in low frequency inductive hyperthermia", *COMPEL – The International Journal for Computation and Mathematics in Electrical and Electronic Engineering*, 31(4), 1096–1104 (2012).

[21] A. Miaskowski, B. Sawicki, and M. Subramanian, "Identification of diffusion coefficients in heat equation on the base of non-adiabatic measurements of ferrofluids", *Proceedings of 2016 17th International Conference Computational Problems of Electrical Engineering (CPEE)*, 1–4 (2016).

[22] E. Kurgan and P. Gas, "Simulation of the electromagnetic field and temperature distribution in human tissue in RF hyperthermia", *Przeglad Elektrotechniczny* 91(1), 169–172 (2015).

[23] B. Mochnacki and M. Ciesielski, "Sensitivity of transient temperature field in domain of forearm insulated by protective clothing with respect to perturbations of external boundary heat flux", *Bull. Pol. Ac.: Tech*. 64(3), 591–598 (2016).